Available online at www.sciencedirect.com

ScienceDirect

Ceramics International 40 (2014) 4681–4690

CERAMICS INTERNATIONAL

www.elsevier.com/locate/ceramint

Bactericidal efficiency of nanostructured Al–O/Ti–O composite thin films prepared by dual magnetron reactive co-sputtering technique

A.B. Panda[a,c], S. Gopikishan[a], S.K. Mahapatra[a], P.K. Barhai[a], A.K. Das[b], I. Banerjee[a,*]

[a]*Department of Applied Physics, Birla Institute of Technology, Mesra, Ranchi 835215, India*
[b]*Laser and Plasma Technology Division, Bhabha Atomic Research Centre, Mumbai 400085, India*
[c]*C.V. Raman College of Engineering, Janla, Bhubaneswar 752054, India*

Received 28 June 2013; received in revised form 30 August 2013; accepted 31 August 2013
Available online 16 September 2013

Abstract

Mixed oxide Al–O/Ti–O composite nanostructured thin films were prepared at Ar:O_2 gas ratio of 70:30 (7:3 in sccm) by reactive magnetron co-sputtering method. The effect of Al in the films on the antibacterial efficiency has been studied. *In situ* optical emission spectra (OES) were recorded in order to study the plasma chemistry as well as nucleation and growth process during deposition. The films were characterised by X-ray diffraction (XRD), inductively coupled plasma optical emission spectrometer (ICP-OES), field emission scanning electron microscope (FESEM), optical contact angle (OCA) and UV–visible transmission spectra (UV–vis). The qualitative and quantitative bactericidal efficiency was studied through SEM image of the treated *E. coli* cells (*Escherichia coli NCIM 2809*) and optical density (OD) measurement using UV–vis spectrometer, respectively. The better bactericidal efficiency was observed in the film with more Al content. The crystallinity, surface chemical composition, band gap in context of Al present in the films were discussed and correlated to bactericidal efficiency in the light of *in situ* investigation of plasma from OES.

Keywords: TiO_2 films; Bactericidal efficiency; Plasma parameters; Al–O/Ti–O composite films

1. Introduction

Bio-compatible, non-toxic, wide band gap semiconductors like titanium dioxide thin films are extensively studied for photo killing of bacteria for environmental purification (water and air purification) soon after the discovery of Honda–Fujisima effect [1]. Antibacterial and photocatalytic properties of the films strongly depend on the microstructure, particle size, band gap, film thickness, hydrophilicity of the deposited films. Photocatalysis proceeds with the electron–hole pair formation via UV irradiation followed by their separation to form reactive species like $OH^{\cdot}$, O_2^{-}, HO_2, H_2O_2, etc. Attempts have been made by various researchers to enhance effective photocatalysis through suitable doping of various metals (Cu, Co, Ni, Cr, Au, Ag, Pt, etc. transition metals) and non-metals (N, S, C, B, etc.) in TiO_2 [2–9]. Studies related to alumina doped TiO_2 have proved to be a good candidate of photocatalysis [10,11]. Basically TiO_2 behaves as the photocatalytic sites generating electron–hole pairs under irradiation whereas Al_2O_3 provides better adsorption sites in the vicinity of TiO_2 by increasing the effective surface area. However, the percentage of TiO_2 and Al_2O_3 greatly influences the photocatalytic activity of the mixed materials [12].

Among other methods, sputtering techniques provide large area uniformity of film thickness and strong adhesion to substrate. Moreover, we can control the structure, composition of the deposited species easily by adjusting the deposition–condition parameters such as working pressure, power, time of deposition, substrate temperature and distance to the target and partial pressure of reactive and sputtering gasses, etc. [13–15]. In this present work, mixed oxide Al–O/Ti–O composite nanostructured thin films were deposited with two Ti and Al targets connected to constant RF and varying DC powers, respectively, in an argon–oxygen environment. The novelty of

*Corresponding author. Tel.: +91 651 2275402; fax: +91 651 2275401.
E-mail address: indranibanerjee@bitmesra.ac.in (I. Banerjee).

0272-8842/$ - see front matter © 2013 Elsevier Ltd and Techna Group S.r.l. All rights reserved.
http://dx.doi.org/10.1016/j.ceramint.2013.08.141

the work is to investigate the complex plasma chemistry affecting the nucleation and growth of the thin films during deposition. *In situ* measurement of plasma process parameters such as electron temperature, electron and ion velocities has been estimated through optical emission spectroscopy (OES) [16,17]. A correlation of microstructure, optical band gap, hydrophilicity to that of antibacterial properties is explained of the mixed oxide films in the light of gas phase understanding.

2. Experimental details

2.1. Preparation of thin films and in situ study of sputtered species through OES

Four nanostructured mixed oxide Al–O/Ti–O thin films were prepared on glass, quartz and silicon substrates in an argon and oxygen atmosphere by reactive magnetron co-sputtering system at a constant Ar:O_2 gas ratio of 70:30 (that is 7 sccm of Ar and 3 sccm of oxygen). For optical properties like transmittance of the films quartz substrates were being used because of its non-absorbance of light photons below 400 nm unlike glass substrates. For bactericidal studies usually glass substrates were used and for rest characterizations silicon substrates were used. Dual-magnetron tilted at an angle 45° to each other having ring-type permanent magnet was used with closed magnetic field. Fig. 1 shows the schematic diagram for the co-sputtering unit. The system consists of a chamber coupled with diffusion and rotary vacuum system, capable of producing vacuum up to $\sim 10^{-6}$ mbar. The chamber is provided with two planar unbalanced magnetrons (2 in. dia) having polarity of the magnets opposite to each other, thus forming a dual magnetron closed $\vec{\mathbf{B}}$ field deposition unit. One of the magnetrons is connected to the variable RF power supply up to 600 W with a constant frequency of 13.56 MHz whereas another magnetron is connected to the variable DC power supply up to 1000 W. Both the magnetrons were water cooled during the deposition period. Before each run, the chamber was pumped down to 10^{-5} mbar and the target was pre-sputtered in pure argon atmosphere for 30 min in order to remove the surface oxide layer of the target. After that, spec pure oxygen along with argon was introduced at the defined ratio by MKS mass flow controller into the chamber maintaining a constant working pressure of 10^{-2} mbar. Prior to deposition the substrates were ultrasonicated by acetone for 30 min. For the deposition of films, titanium target (99.99% purity) was mounted on the magnetron connected to RF power supply and aluminium target (99.99% purity) was mounted on the magnetron connected to the DC power. The DC was varied as 0 W (magnetron containing Al target was switched off), 15 W, 30 W and 45 W whereas RF power was kept constant at 200 W. The films were labelled as S_0, S_1, S_2 and S_3. The substrate to target distance (50 cm), the working pressure ($\sim 5 \times 10^{-2}$ mbar) and time of deposition (1 h) were kept fixed for all the samples to deposit.

Quartz window view port in the chamber wall was coupled with spectrometer (Get Spec UV/vis 0172 grating UA, 200–

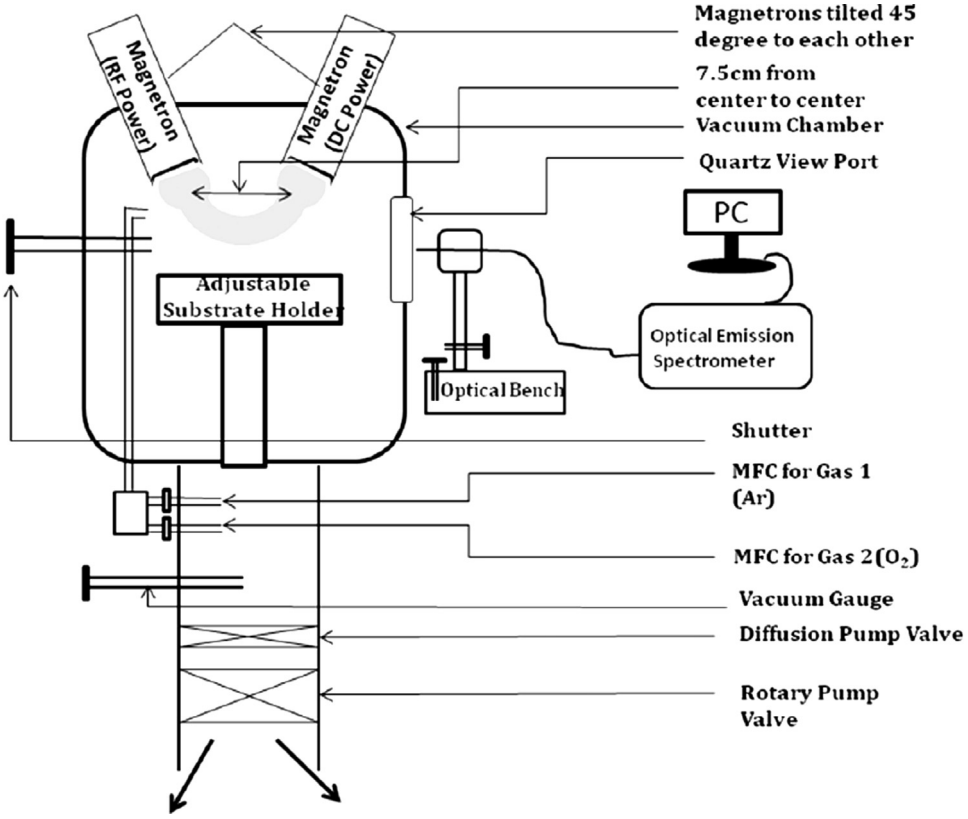

Fig. 1. Schematic diagram of reactive dual-magnetron co-sputtering unit with closed magnetic field.

720 nm, CCD detector with 3648 pixels, 10 μm entrance slit and spectral resolution of 0.27 nm) through optical fiber. The space integrated emission spectra were recorded during the deposition of each sample at the near target position, where the plasma emission was intense.

2.2. Characterisation of the thin films

The thickness of the as-deposited films was measured using the Ellipsometric technique. The crystallinity and phase of the as-deposited films were studied through Grazing Incidence X-ray diffractometer (GIXRD, Model PW-1840- PHILIPS) using Cu Kα ($\lambda = 1.5418$ Å) as the source. The surface morphology of the films was studied using FESEM (ZEISS). The amount of Al and Ti was estimated from Inductively Coupled Plasma-Optical Emission Spectrometry (ICP-OES, Perkin–Elmer). For this purpose, the weights of the deposited thin films on glass substrates were measured before putting into concentrated H_2SO_4 maintained at 60–70 °C for 5–10 min. The glass substrates were then removed from the solution and weighted again. The volume of the solutions was made up to100 ml by adding deionised water. The solutions were then subjected to the ICP chamber for measuring the amounts of metal (Al and Ti) in parts per million (ppm) and converted to mg/l for each film. The amount of materials in mg for 100 mg of film materials for each film was estimated from the difference in weights before and after dissolution of the films. The UV–vis transmission spectra were recorded for the films deposited on quartz substrates in a Perkin–Elmer LAMBDA-25 spectrometer from which the optical band gaps were determined. To examine the photoinduced hydrophilicity, the as-deposited films on glass substrates were illuminated by a UV lamp of power 400 W/cm^2 for 30 min. The optical contact angles were measured using a Data Physics, Germany OCAH 230 system.

2.3. Experimental procedure to study bactericidal efficiency

Antibacterial activity of the as-deposited films was performed under UV (400 W, medium pressure mercury lamp, wavelength 200–400 nm with peaks at 254, 356, 365 nm) irradiation with thin films kept at 50 cm distance from the lamp. *E. coli* (gram-negative *Escherichia coli NCIM 2809*) was used as model bacteria. The light intensity was measured to be 40 W/cm^2 at the sample position. The equipments including thin films were washed out with distilled water and autoclaved at 121.5 °C, 15 psi for 30 min under sterilisation. *E. coli* bacteria were grown in a 20 ml of nutrient broth at 37 °C for 12–14 h maintaining a pH of 7–7.2. Biocidal efficiency of the deposited films was studied by film pour method similar to 3 cm^3 test as reported by Krysa et al. [18]. All the four as-deposited sterilised films were positioned in four beakers containing 20 ml of cultured *E. coli* solution each and were placed on magnetic stirrers. The magnetic needles were set to a very low rotation (20 rpm) to set the whole of the bacterial suspension under uniform contact to the surface of thin films. After each 1 h of UV irradiation, the treated solutions with and without films were washed by centrifuging at 10,000 rpm for 20 min in 20 °C. The centrifuged cells are then re-suspended and diluted to 10^{-1}–10^{-5} in test tubes for different concentrations. For the qualitative investigation of the ruptured E.coli cells, 2 μl of the diluted cell solution of different concentrations were drop coated on clean sterilized silicon (10 mm×10 mm) substrates. The substrates were dried at room temperature in a sterilised environment. These samples were then visualised under scanning electron microscope (SEM). In order to quantify the bactericidal efficiency of the films, 1.5 ml of the treated solutions (without centrifuge) were taken in quartz cuvet, and absorption spectra were recorded using the UV–vis spectrometer. The optical density (OD) was then determined from the absorbance recorded at 600 nm.

The same procedure was also followed for the qualitative and quantitative analysis of post-UV (the above mentioned specification) irradiated films for 30 min. The results for both as-deposited and post-UV irradiated films were then compared.

3. Results and discussion

3.1. Optical emission spectroscopic study of film deposition

The deposition of thin films in the reactive magnetron sputtering is based on the solid–vapour interaction mechanism. The vapour of metals sputtered (in our case Al and Ti) reacts with the ambient oxygen to form their respective oxides inside plasma. The compounds formed in the plasma get deposited on substrates through momentum transfer undergoing heterogeneous nucleation. The species such as sputtered particles from Ti and Al targets, any combinations of Ti_xO_{2-x} and Al_2O_{3-x} molecules, energetic e^-, +ve ions, O^- and neutrals reflected from target (Ar and O_2) are the main constituents of plasma species [19–21]. However, for closed magnetic field dual magnetron sputtering, the plasma confinement is enhanced by an electrostatic confinement and most of the magnetron cathodes repelled electrons oscillate between them [22]. Most of the electrons reside near the cathode and most of the collisions occur in this region due to strong magnetic trap. The electrons originating due to co-sputtering overlap between two magnetron regions [21]. This causes increased ionisation of sputtering and reactive gases in the vicinity of target regions enhancing sputtering rates from targets. The ionisation of reactive gas particles (here oxygen) also increases the probability of bond formation with the sputtered metal species (Ti and Al) resulting into denser film formation [21]. We can realise the above phenomena by examining the recorded emission spectra of various species through OES.

Fig. 2(a) and (b) shows the line of sight space integrated spectra for the plasma during film deposition in the range $\lambda = 300$–600 nm and $\lambda = 600$–750 nm, respectively. The figure shows that the atomic characteristic emission lines of Ar I, Ti I and Al I dominate the spectrum (Table 1 as per NIST data). Emission lines corresponding to the O I are not observed in the spectra due to their relatively small intensities as compared to the metal lines [23]. As expected, the intensities of the lines of Ar I and Al I increase and Ti I decrease for samples S_1, S_2 and S_3. The OES data are well in agreement with the elemental analysis of Ti and Al from ICP-

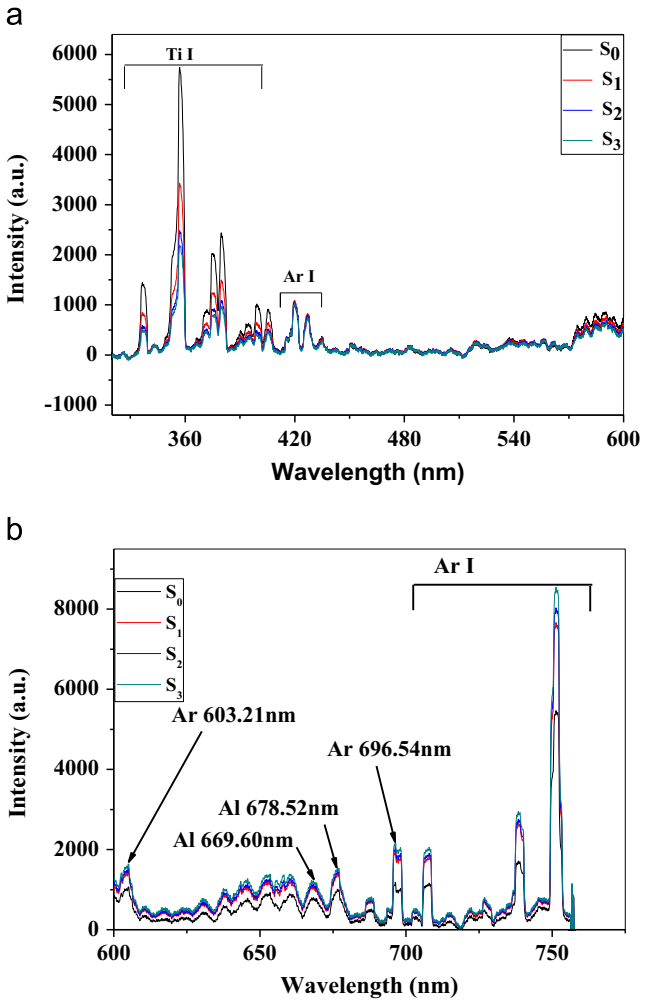

Fig. 2. *In situ* optical emission spectra recorded during the deposition of S_0, S_1, S_2 and S_3 films (a) in the range of wavelength 320–600 nm and (b) in the range of wavelength 600–775 nm.

Table 1
Observed emission lines details from recoded OES spectra (NIST database).

Species	Emitted wavelength (λ in nm)	Spectroscopic terms for transition	Upper level energy (E in eV)
Ti I	336.90	a ^{3}F– x ^{5}D°	3.72
Ti I	357.42	b ^{1}G–u ^{1}G°	5.73
Ti I	375.28	a ^{3}F–x ^{3}F°	3.35
Ti I	379.83	–	–
Ti I	393.42	a ^{3}F–y ^{5}D°	3.19
Ti I	398.97	a ^{3}F–y ^{3}F°	3.12
Ti I	405.502	a ^{3}P–x ^{3}P°	4.1
Ar I	420.06	[3/2]°–[5/2]	14.49
Ar I	427.21	^{2}[3/2]°–^{2}[3/2]	14.52
Ar I	603.21	^{2}[5/2]°–^{2}[7/2]°	15.13
Al I	669.54	^{2}S–^{2}P°	4.99
Al I	678.52	^{2}D–^{2}F°	5.84
Ar I	696.54	^{2}[3/2]°–^{2}[1/2]	13.32
Ar I	706.72	^{2}[3/2]°–^{2}[3/2]	13.30
Ar I	751.46	^{2}[3/2]°–^{2}[1/2]	13.27

OES and XRD spectra, which is discussed later in this paper. Fig. 3 shows the Al–O and Ti–O band intensities recorded during the successive deposition of S_0, S_1, S_2 and S_3 films. Ti–O band heads were formed at λ=586.17 nm (ν'=2, ν''=4), λ=581.0 (ν'=1, ν''=3) and λ= 575.8 nm (ν'=0, ν''=2) along with band heads corresponding to Al–O at λ= 516.08 nm (ν'=4, ν''=5) and λ=484.21 (ν'=2, ν''=2). This signifies the formation of oxide or suboxides of both Ti and Al during deposition. Inset of Fig. 3 presents the variation of ratio of area under the Ti–O strongest band head at λ=586.17 nm (ν'=2, ν''=4) to the area under Al–O strongest band head at λ= 516.08 nm (ν'=4, ν''=5) during deposition. It could be observed that Ti–O formation gradually decreases with the increase in the Al–O formation which was controlled through the DC power fed to the magnetron containing Al. The percentage of Al–O as recorded varied from 8 to16% for the films. However, interestingly for S_0 weak signals of Al I and Al–O were also recorded though the supply for Al was made absent. This is attributed to dual magnetron closed magnetic field discharge phenomena. The electrons and ions originating from Ti target magnetron induce sputtering from Al target even though the magnetron for the Al target was kept in switched off mode. In the present system, the magnetrons are separated at 7.5 cm and tilted at 45° to each other which is within the plasma preview. The photographs in Fig. 4(a) and (b) clearly demonstrate these above phenomena with both the magnetrons at switched on or one of them in switched off respectively.

Plasma used here for sputtering is low pressure, glow discharge plasma. In order to understand the complex plasma chemistry responsible for the film formation, the electron temperature was estimated by relative intensity method. The plasma has been assumed to be in partial local thermodynamic equilibrium (PLTE). The following formula was used for calculating the electron temperature [17,24]:

$$T_e = \frac{E_m - E_p}{k \ln\left(\frac{I_{pn} A_{ms} g_m \lambda_{pn}}{I_{ms} A_{pn} g_p \lambda_{ms}}\right)} \quad (1)$$

where I_{ms} and I_{pn} are the measured intensities from m–s and p–n transitions, respectively. A_{ms} and A_{pn} are the transition probabilities, λ_{ms} and λ_{pn} are wavelengths, E_m and E_p are the upper level energies, g_m and g_p their statistical weights (determined from NIST data) and k is the Boltzmann constant.

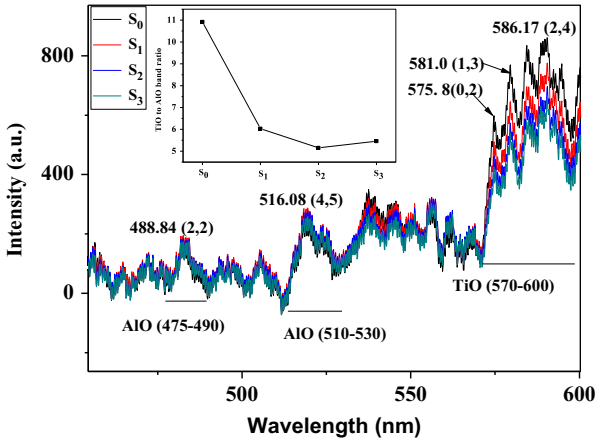

Fig. 3. Al–O and Ti–O band intensity recorded during the successive deposition of S_0, S_1, S_2 and S_3 films. Inset presents the variation of Ti–O to Al–O band ratios of strongest band heads (λ=586.17 nm for Ti–O and λ=516.08 nm for Al–O) during the deposition of these films.

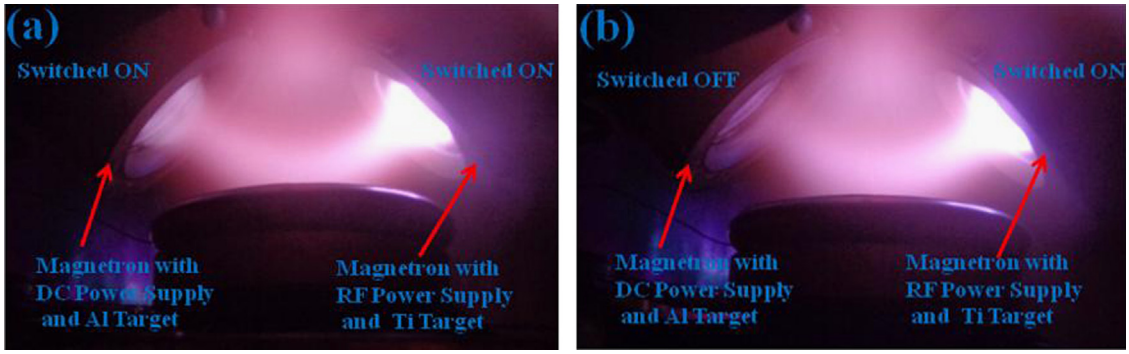

Fig. 4. Geometry of the discharge in the plasma chamber (a) when both the magnetrons were switched on and (b) magnetron connected to DC power supply was switched off during the deposition of films.

Eq. (1) indicates that, in order to get a functional that is sensitive to T_e, it is desirable to select two excited states with E_m–E_p comparable to T_e i.e., 1–4 eV in low pressure, low temperature plasmas [16]. For the lines for which the difference in energy levels is much smaller than that of T_e, the ratio may be independent of T_e. Therefore, the emission lines λ_{ms}=603.21 nm and λ_{pn}=696.54 nm of Ar I were used for T_e determination. Since the PLTE model is only an assumption, the electron temperature obtained from this method was only an approximation [17]. The electron temperatures found by the above formula were 4.581, 3.005, 3.043, and 3.058 in eV for the deposition of samples S_0, S_1, S_2 and S_3, respectively. The estimated temperature range is well in agreement with the reported value for the RF, DC plasmas used for the sputtering system [16]. The electron temperature decreases from 4.581 to 3.005 eV as soon as the DC bias is switched on from 0 to 15 W. However, the electron temperature seems to be almost constant for S_1, S_2 and S_3.

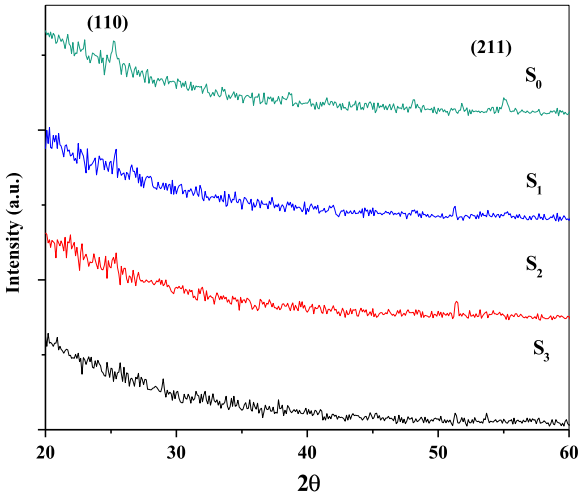

Fig. 5. GIXRD patterns of the films with varying DC power supply magnetron having Al target.

3.2. Film characteristics

The thickness of the films was measured to be 284, 298, 312 and 325 nm for the samples S_0, S_1, S_2, and S_3, respectively, as measured from the ellipsometer. The increase of the thickness is due to the increase of DC power to the magnetron with Al target causing more sputtering in the system.

Fig. 5 shows the GIXRD patterns of the films with scanning speed and the incident angle of the radiation to be 4° min^{-1} and 3°, respectively. The small peak at 2θ ~27° and a small peak at ~55° belongs to rutile phase (110) and (211) (JCPDS no. 88-1175 and 84-1286) of TiO_2, respectively. The intensity of the TiO_2 peaks decreases consequently for film S_0, S_1 and S_2 and completely disappears in S_3. However, no traces of unreacted Al or Al_2O_3 were observed. Such XRD pattern is explained from *in situ* measurements through OES. The subsequent addition of Al atoms or ions to the plasma volume during the deposition of films S_0, S_1, S_2 and S_3 lowers the ambient temperature which hinders the crystallisation of TiO_2. Moreover, the crystallisation temperature (900 °C) and enthalpy of formation (−1625 kJ/mol) for Al_2O_3 being much higher than TiO_2 (330 °C and −944.74 kJ/mol) probably prohibit crystallisation of aluminium [25]. However, the emission lines of Al–O bands observed in the OES spectra (Fig. 3) indicate the formation of oxides and suboxides of aluminium in the amorphous form in the film. The elemental analysis of Ti and Al present in the films was done through ICP-OES and shown in Fig. 6. The XRD results resemblance the elemental analysis achieved from ICP-OES.

The Al content in 100 mg of the film materials varies from 0.35% to 3.51%. The percentage of Al content < 10% in TiO_2 has been proved to be better photocatalytic reported later in this paper [12].

The surface morphology of the deposited films was observed through FESEM micrographs and shown in Fig. 7. The films with higher Al content show less globular morphology having disordered surface with smaller particle sizes. Sample S_0 with less Al indicates more defined structural characteristics whereas other samples with more Al show flake-like structures. The films are composed of irregular grains of different sizes with only few pores. Similar morphology in Al-doped TiO_2 nanoceramic and Al_2O_3-doped thin films has been reported in the literature [26–28].

Fig. 8 shows the optical transmission spectra for the films in the UV–vis range as a function of Al content in the films. The

transmittance of the samples S_2 and S_3 is almost 80% and for films S_0 and S_1 it is around 90% i.e., T % decreases with increase in Al content. However, no orderly edge shift in accordance with the Al content is observed. Also it can be depicted from the figure that the fundamental edge shift for films S_0 and S_1 to higher wavelengths i.e., red shift occurs. The difference in the average transmittance nature of such type is also due to the thickness (from samples S_0 to S_3) and other film properties like structure, composition and surface morphology [3]. The increase in Al in the films makes the morphology more disordered and amorphous. This increases the film roughness, for which the light reflect and interfere causing less transmittance and edge shift towards the UV range. These are in agreement with both the XRD and FESEM results shown above.

The absorption for all the samples occurs at wavelength around 300–330 nm with an abrupt change of transmittance. The optical band gaps for all films were calculated using the following Tauc equation [29]:

$$(\alpha h\nu) = A(h\nu - E_g)^n, \quad \alpha = d^{-1}\ln(1/T) \tag{2}$$

where $h\nu$ is the excitation photon energy, E_g is the optical band gap, A is a constant which is independent on $(h\nu)$ and α is the absorption coefficient. For $n=2$ fitting, the band gap is supposed to be indirect and for $n=1/2$ the fitting is direct.

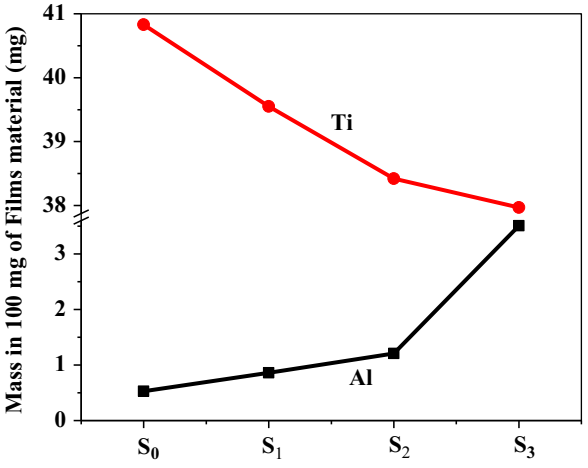

Fig. 6. The amount of titanium and aluminium in 100 gm of film materials as estimated from ICP-OES.

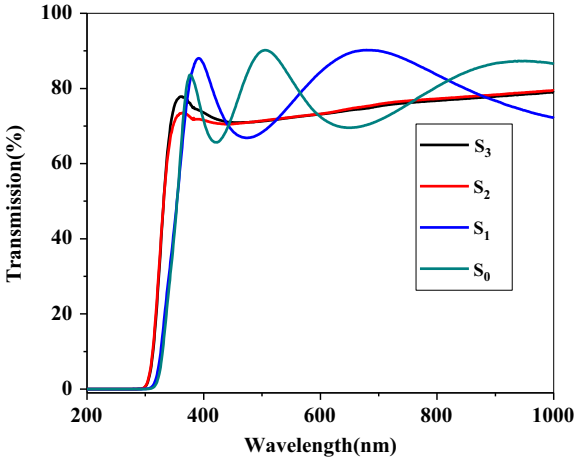

Fig. 8. Optical transmission spectra in the UV–vis range as a function of DC power to magnetron having Al target.

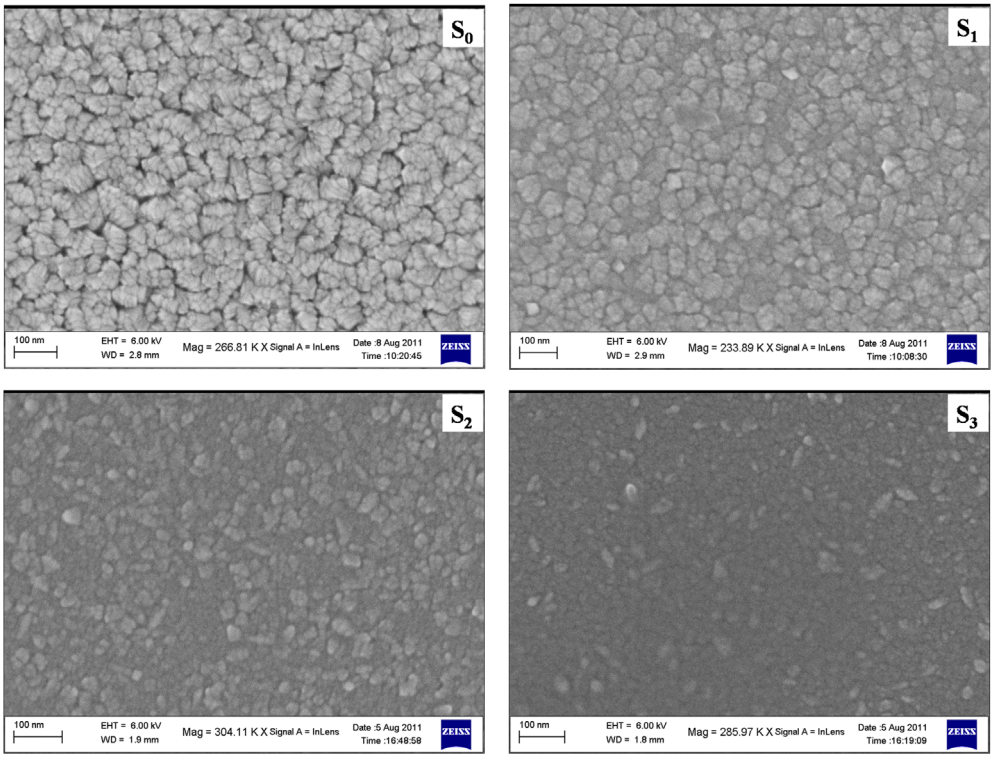

Fig. 7. Surface morphology of the films as observed from FESEM micrographs with increasing DC power supply to magnetron having Al target.

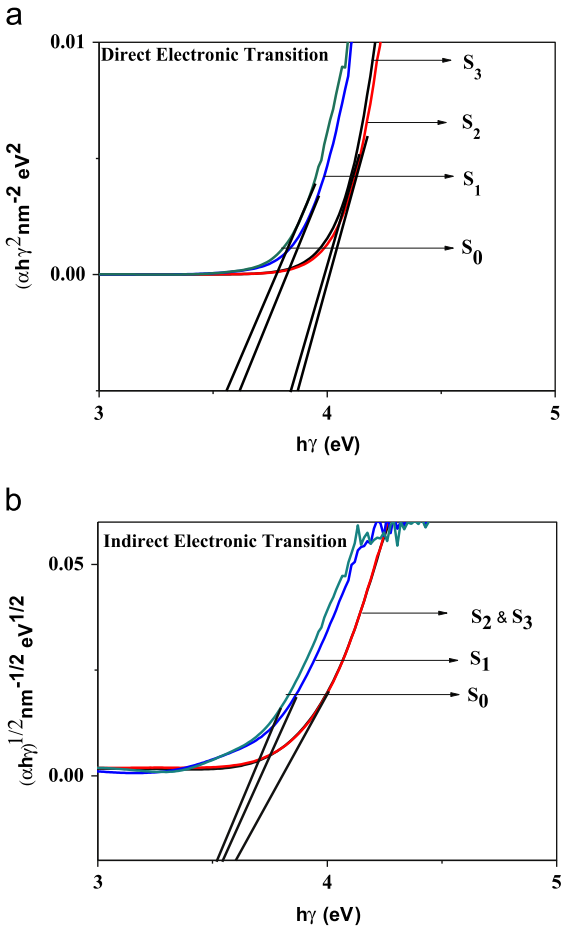

Fig. 9. Band gaps: (a) direct band gap and (b) indirect band gap as a function of DC power to magnetron having Al target.

Fig. 9 depicts both direct and indirect fundamental interband electronic transitions for $n=1/2$ and 2, respectively. The possibility of determining both direct and indirect energy band gaps in the same sample might be attributed to the combined effect due to the formation of mixed oxide of Al–O/Ti–O composite materials as confirmed from OES spectra [30]. Such possibilities might also arise due to the existence of mixed phases in the material. However, the diffraction pattern (Fig. 5) shows that the films to be mostly amorphous with very weak crystallinity. Moreover, the actual determination of the type of band gap in a mixed oxide compound is more critical and needs further investigation [30]. Fig. 9 shows that in both direct and indirect transitions the band gaps for the samples S_0, S_1, S_2, and S_3 are 3.54, 3.61, 3.83, and 3.86 eV and 3.50, 3.53, 3.59 and 3.59 eV, respectively, by extrapolating the straight line portion to the energy axis. For both the calculations, the band gaps of the films S_1, S_2, and S_3 are higher than that of S_0 which resemblance with some of the earlier studies [10,31]. The increase of band gap can be explained due to the fact that the band gap of Al_2O_3 is higher than that of TiO_2. Hence, the band gaps of mixed films were observed to increase. Moreover, the quantum size effect described in our earlier publication [32] and justified by the FESEM micrograph as shown in Fig. 7 may be another reason.

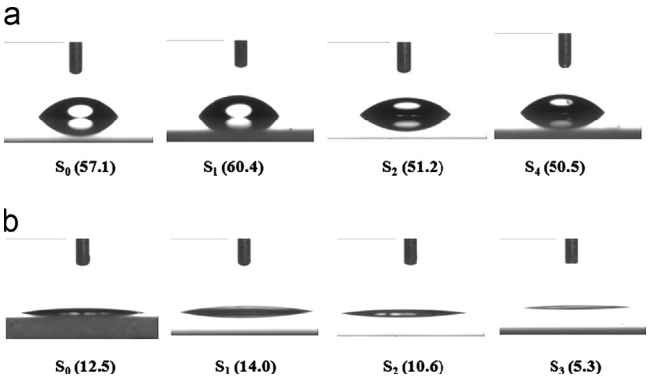

Fig. 10. Optical contact angle images with water of (a) as-deposited and (b) UV irradiated films for 30 min as a function of DC power to magnetron having Al target.

Increased band gap in the films enhances the photocatalysis and hence its bactericidal efficiency. However, hydrophilicity of the films is another deciding factor for photocatalytic efficiency. Fig. 10(a) represents the optical contact angle for the as-deposited thin films. The as-deposited films showed less hydrophobic nature with almost same contact angles for all the samples. These low contact angles are due to the absorbed surface hydroxyl groups on the deposited film surfaces. This shows that the oxygen of titania film surface deposited by magnetron sputtering is unsaturated which leads to high surface energy and unbalanced surface charges. Therefore, in order to balance the surface charges, some polar molecular ions (e.g., H_2O) get absorbed. This chemical absorption of water on the surface generates OH• through hydrolysis. This lowers the contact angle of the films [32,33]. The hydrophilicity of as-deposited films was further enhanced through UV irradiation for 30 min and reported in Fig. 10(b). The decrease in contact angles and increase in hydrophilicity was observed for the films with increasing Al content (Fig. 10(b)). The transition from the hydrophobic to hydrophilic states may be connected to photoactive electronic transition across the energy gap. This reduces the surface Ti^{4+} sites to Ti^{3+} accompanying oxygen vacancy and adsorption of dissociative water on these sites [11,34]. The Al content films cause substitution of Ti^{4+} with Al^{3+} on account of smaller ionic radius of Al^{3+} than Ti^{4+}. To compensate a larger ionic radius than Ti^{4+}, Ti^{3+} is required. Thus Ti^{3+} concentration increases making the films hydrophilic. Also the formal charge formed due to substitution of Ti^{4+} with Al^{3+} may be compensated via the formation of O^- to O^{2-} leading to oxygen vacancies. This also helps the films to be more hydrophilic in nature [35]. Moreover, the surface acidity also affects the hydrophilicity of the films which may increase or decrease with the dopant materials and concentration [11].

3.3. Study of bactericidal efficiency of the films

The qualitative analysis of the bactericidal efficiency of the films was studied through SEM images of the treated and untreated *E. coli* cells. Fig. 11(a) and (b) shows the scanning

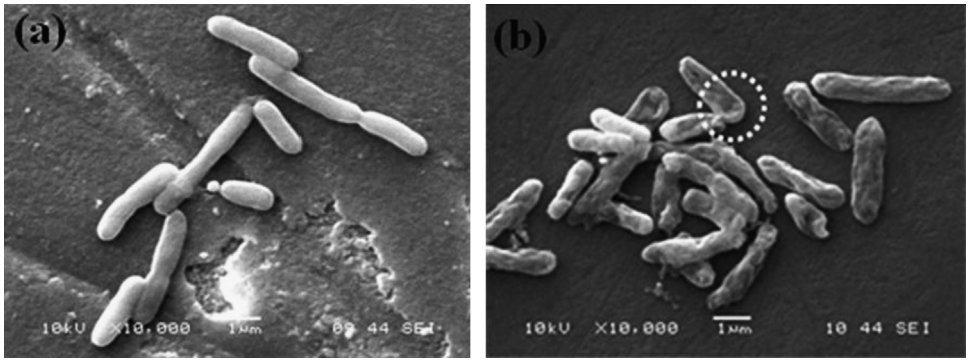

Fig. 11. Scanning electron microscope image of (a) virgin *E. coli* cells and (b) film treated *E. coli* cells under 2 h of UV irradiation.

electron microscope image of both virgin *E. coli* and film treated *E. coli* under 2 h of UV irradiation, respectively. Fig. 11(a) shows the picture of the fully grown rod shaped virgin *E. coli* cells cultured in nutrient broth. Fig. 11(b) shows the ruptured *E. coli* cells. The outer membrane damage has been marked by dotted circle. This is a direct evidence of destruction of endotoxin, an integral component of the outer membrane under UV irradiation in the presence of the films. The cell deformation causing its death due to TiO_2 films can be explained through two mechanisms. The highly reactive species (ROS) such as OH•, O_2^-, HO_2•, H_2O_2 in aqueous medium like water are formed via the photo excited electron (e^-) and hole (h^+) in its conduction and valence bands of TiO_2. The ROS react with the outer cell membrane (beyond the peptidoglycan layer containing phospholipids, protein and lipopolysaccharide (LPS) as major constituents) and changes its permeability. The ROS enter into the cytoplasm leading to the peroxidation of membrane lipid causing the death of the cells [36–38]. Another mechanism may be attributed to the lipid peroxidation reaction leading to the mal functioning of survival activities like respiration of the organisms [39,40].

The quantitative analysis of the bactericidal properties of as-deposited and 30 min post-UV irradiated films S_0, S_1, S_2 and S_3 is shown in Fig. 12(a) and (b), respectively. The optical density (OD) of the incubated cells after film treatment at 600 nm absorbance gives the quantitative analysis of the cells surviving after photocatalysis. This spectroscopic analysis is the fastest method than the standard or viable count and inhabitation zone of bacteria methods described in the literature [41]. The optical densities of control cells (mother culture) and only UV irradiated (without films S_0, S_1, S_2 and S_3) cells of same incubation time were also taken for comparison. This shows that the optical density and hence the number of bacterial cell decreases as compared to the control and only UV irradiated. The decrease in OD and hence the lesser bacterial survival rate were noticed for the cells in the presence of films S_0, S_1, S_2, and S_3. Inset figures show the antibacterial efficiency of the samples taking the OD of the mother culture (MC) as our initial count. The percentage of antibacterial efficiency increases for both as-deposited and post-irradiated films with the increase of Al content. This activity of the decrease in survival rate is attributed to the incorporation of Al_2O_3 or its suboxides (0.5–3.5% by weight of Al as measured

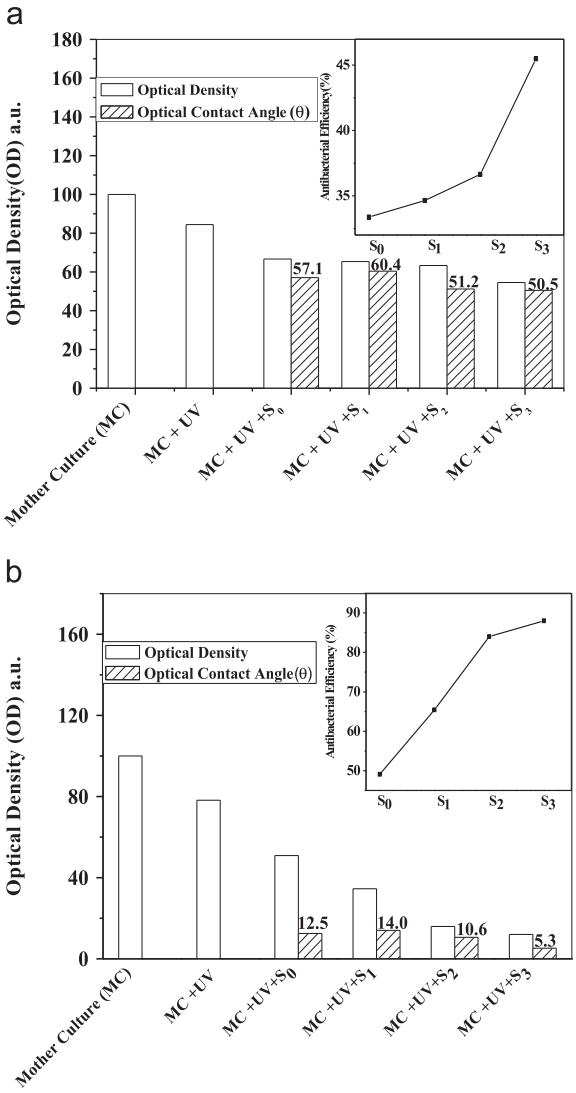

Fig. 12. Quantitative analysis of bactericidal properties of (a) as-deposited and (b) 30 min post-UV irradiated films S_0, S_1, S_2 and S_3 under UV irradiation with optical contact angle for 4 h. The inset graph shows the antibacterial efficiency of the respective films.

from ICP-OES) to the films. The literature reveals [12] that the BET surface area of TiO_2 increases from $\sim$50 m^2/g to $\sim$200 m^2/g for $<$ 10% mixing of Al_2O_3. This increase in effective surface area increases the adsorption ability of the

mixed oxide materials of (Al_2O_3/TiO_2). Al_2O_3 in the vicinity of TiO_2 adsorbs more solution materials i.e., provide pre-concentration of materials to the nearby photoactive site of TiO_2 for decomposition. Moreover, Al_2O_3 can also adsorb material even in the dark which could later be decomposed by TiO_2 under UV irradiation. The increase in band gap, photoinduced hydrophilicity and small grain size also assist the antibacterial property. The higher band gap provides higher reduction potential to the photogenerated electrons to get converted to oxygen or dioxygen to superoxides (O_2^-) or even to hydrogen peroxide (H_2O_2) in aqueous environment [42]. The smaller grain size increases the reactive surface area. The relation of increase in photoinduced hydrophilicity to the bactericidal efficiency is reflected in Fig. 12(b). The percentage of antibacterial efficiency reached was 45% for as-deposited films. On the other hand, for the same films it was noticed to be 90% after 30 min of UV treatment before performing photocatalysis. The 30 min of UV treatment caused abrupt change of optical contact angle towards more hydrophilic surface. This favours the photocatalytic effect as large area of the films comes in contact to the aqueous environment thus increasing the reaction sites for the process.

4. Conclusion

The present paper involves investigation of bactericidal properties of the mixed oxide composite thin films with varying composition of Al_2O_3 in TiO_2. Understanding of the plasma induced gas phase growth of the mixed oxide has been done using *in situ* optical emission spectroscopic measurements. The presence of Al_2O_3 in TiO_2 enhanced the bactericidal efficiency of the films. Such systematic study could be highly informative and can be useful for the synthesis of highly efficient bactericidal films.

Acknowledgements

The authors wish to acknowledge BRNS, DAE, India, for funding the project under which the work has been performed. The authors also wish to acknowledge Pharmacy Department of B.I.T. for providing the *E. coli* cells for bactericidal experiments.

References

[1] A. Fujishima, K. Honda, Electrochemical photolysis of water at a semiconductor electrode, Nature 238 (1972) 37–38.
[2] A. Fujishima, T.N. Rao, D.A. Tryk, Titanium dioxide photocatalysis, Journal of Photochemistry and Photobiology C: Photochemistry Reviews 1 (2000) 1–21.
[3] S. Serio, M.E. Melo Jorge, M.J.P. Maneira, Y. Nunes, Influence of O_2 partial pressure on the growth of nanostructured anatase phase TiO_2 thin films prepared by DC reactive magnetron sputtering, Material Chemistry and Physics 126 (2011) 73–81.
[4] M. Anpo, Use of visible light. Second-generation titanium dioxide photocatalysts prepared by the application of an advanced metal ion-implantation method, Pure and Applied Chemistry Chimie Pure et appliquée 72 (1) (2000) 787–792.
[5] M.D.H.A. Fuerte, A.J. Maira, A.M. Arias, M.F. Garcia, J.C. Conesa, J. Soria, Visible light-activated nanosized doped-TiO_2 photocatalysts, Chemical Communications 24 (2001) 2718–2719.
[6] H. Yamashita, M. Harada, J. Misaka, et al., Application of ion beam techniques for preparation of metal ion-implanted TiO_2 thin filmphoto-catalyst available under visible light irradiation: metal ionimplantation and ionized cluster beam method, Journal of Synchrotron Radiation 8 (2001) 569–571.
[7] T. Ohno, T. Mitsui, M. Matsumura, Photocatalytic activity of S doped TiO_2 photocatalyst under visible light, Chemistry Letters 32 (2003) 364–365.
[8] Y. Liu, X. Chen, J. Li, C. Burda, Photocatalytic degradation of azo dyes by nitrogen-doped TiO_2 nanocatalyst, Chemosphere 61 (2005) 11–18.
[9] T. Hirai, K. Suzuki, I. Komasawa, Preparation and photocatalytic properties of composite CdS nanoparticles-titanium dioxide particles, Journal of Colloid and Interface Science 244 (2001) 262–265.
[10] S.S. Lin, D.K. Wu, The properties of Al-doped TiO_2 nanoceramic films deposited by simultaneous rf and dc magnetron sputtering, Ceramics International 36 (2010) 87–91.
[11] Y.C. Lee, Y.P. Hong, H.Y. Lee, H. Kim, Y.J. Jung, K.H. Ko, H.S. Jung, K.S. Hong, Photocatalysis and hydrophilicity of doped TiO_2 thin films, Journal of Colloid and Interface Science 267 (2003) 127–131.
[12] C. Anderson, A.J. Bard, Improved photocatalytic activity and characterization of mixed TiO_2/SiO_2 and TiO_2/Al_2O_3 materials, Journal of Physical Chemistry B 101 (1997) 2611–2616.
[13] B. Liu, X. Zhao, Q. Zhao, C. Li, X. He, The effect of O_2 partial pressure on the structure and photocatalytic property of TiO_2 films prepared by sputtering, Materials Chemistry and Physics 90 (2005) 207–212.
[14] S. Serio, M.E.M. Jorge, M.J.P. Maneira, Y. Nunes, Influence of O_2 partial pressure on the growth of nanostructured anatase phase TiO_2 thin films prepared by DC reactive magnetron sputtering, Materials Chemistry and Physics 126 (2011) 73–81.
[15] S.K. Mohamed, O. Kappertz, T.V.L. Pedersen, R. Drese, M. Wutting, Properties of TiO_x coatings prepared by dc magnetron sputtering, Physica Status Solidi (A) 198 (2003) 224–237.
[16] X.M. Zhu, Y.K. Pu, Optical emission spectroscopy in low-temperature plasmas containing argon and nitrogen: determination of the electron temperature and density by the line ratio method, Journal of Physics D: Applied Physics 43 (2010) 403001–403025.
[17] A. Bousquet, L. Spinelle, J. Cellier, E. Tomasella, Optical emission spectroscopy analysis of Ar/N_2 plasma in reactive magnetron sputtering, Plasma Processes and Polymers 6 (2009) 605–609.
[18] J. Krysa, E. Musilova, J. Zira, Critical assessment of suitable methods used for determination of antimicrobial properties at photocatalytic surfaces, Journal of Hazardous Materials 195 (2011) 100–106.
[19] R. Gouttebaron, D. Cornelissen, R. Snyders, J.P. Dauchot, M. Wautelet, M. Hecq, XPS study of TiO_x thin films prepared by d.c. magnetron sputtering in $Ar–O_2$ gas mixtures, Surface and Interface Analysis 30 (2000) 527–530.
[20] H. Toku, R.S. Pessoa, H.S. Maciel, M. Massi, U.A. Mengui, The effect of oxygen concentration on the low temperature deposition of TiO_2 thin films, Surface and Coatings Technology 202 (2008) 2126–2131.
[21] M. Yusupov, E. Bultinck, D. Depla, A. Bogaerts, Behavior of electrons in a dual-magnetron sputter deposition system: a Monte Carlo model, New Journal of Physics 13 (033018) (2011) 1–17.
[22] J. Musil, J. Vlcek, P. Baroch, Magnetron discharges for thin films plasma processing, in: Y. Pauleau (Ed.), Europian Materials Society, Elseivier, London, 2006, pp. 67–110.
[23] W.D. Sproul, D.J. Christie, D.C. Carter, Thin Solid Films 491 (2005) 1–17.
[24] G. Zambrano, H. Riascos, P. Prieto, E. Restrepo, A. Devia, C. Rincon, Optical emission spectroscopy study of r.f. magnetron sputtering discharge used for multi layers thin film deposition, Surface and Coatings Technology 172 (2003) 144–149.
[25] N.V. Kulkarni, S. Karmakar, I. Banerjee, S.N. Sahasrabudhe, A.K. Das, S.V. Bhoraskar, Growth of nano-particles of Al_2O_3, AlN and iron oxide with different crystalline phases in a thermal plasma reactor, Materials Research Bulletin 44 (2009) 581–588.

[26] S.S. Lin, D.K. Wu, Enhanced optical properties of Al-doped TiO_2 thin films in oxygen or nitrogen atmosphere, Applied Surface Science 255 (2009) (8654-8559).
[27] E.B. Ledesma, M.L.G. Benjume, I.E. Cabrera, A.B. Patino, F.J. E. Beltrán, J. Mostaghimi, M.E.C. García, Photocatalytic activity of Al_2O_3-doped TiO_2 thin films activated with visible light on the bacteria *Escherichia coli*, Materials Science and Engineering: B 174 (2010) 74–79.
[28] K.L. Chopra, Thin Film Phenomena, second ed., Robert E Krieger, New York, 1979.
[29] Z. Qing-nan, L. Chun-ling, L. Bao-shun, Z. Xiu-jian, UV–vis and phtoluminscent of spectra TiO_2 films, Journal of Wuhan University of Technology: Materials Science Edition 18 (2003) 36–39.
[30] K. Morita, G. Mera, K. Yoshida, Y. Ikuhara, A. Kleine, H.J. Kleebe, R. Riedel, Solid State Sciences 23 (2013) 50–57.
[31] B.C. Mohanty, Y.H. Jo, D.H. Yeon, I.J. Choi, Y.S. Cho, Stress-induced anomalous shift of optical band gap in ZnO:Al thin films, Applied Physics Letters 95 (2009) 062103-062105.
[32] A.B. Panda, S.K. Mahapatra, P.K. Barhai, A.K. Das, I. Banerjee, Understanding of gas phase deposition of reactive magnetron sputtered TiO_2 thin films and its correlation with bactericidal efficiency, Applied Surface Science 24 (2012) 9824–9831.
[33] B. Liu, X. Zhao, Q. Zhao, C. Li, X. He, The effect of O_2 partial pressure on the structure and photocatalytic property of TiO_2 films prepared by sputtering, Materials Chemistry and Physics 90 (2005) 207–212.
[34] T. Watanable, A. Nakajima, R. Wang, M. Minabe, S. Koizumi, A. Fujishima, K. Hashimato, Photocatalytic activity and photoinduced hydrophilicity of titanium dioxide coated glass, Thin Solid Films 351 (1999) 260–263.
[35] C.Y. Tsai, H.C. Hsi, H. Bai, K.S. Fan, H.D. Sun, Single-step synthesis of Al-doped TiO2 nanoparticles using non-transferred thermal plasma torch, Japanese Journal of Applied Physics 51 (2012) (01AL01–01AL06).
[36] P.C. Maness, S. Smolinski, D.M. Blacke, Z. Huang, E.J. Wolfrum, W. A. Jacoby, Bactericidal activity of photocatalytic TiO(2) reaction: toward an understanding of its killing mechanism, Applied and Environmental Microbiology 65 (1999) 4094–4098.
[37] Z.X. Lu, L.Z.Z.L. Zhang, W.L. Shi, Z.X. Xie, H.Y. Xie, D. Pang, P. Shen, Cell damage induced by photocatalysis of TiO_2 thin films, Langmuir 19 (2003) 8765–8768.
[38] K. Sunada, T. Watanabe, K. Hashimoto, Studies on photokilling of bacteria on TiO_2 thin film, Journal of Photochemistry and Photobiology A: Chemistry 156 (2003) 227–230.
[39] T. Matsunga, R. Tomada, T. Nakajima, H. Wake, Photochemical sterilization of microbial cells by semiconductor powders, Microbiology Letters 29 (1985) 211–214.
[40] T. Matsunga, R. Tomada, Y. Nakajima, N. Nakamura, T. Komine, Continuous-sterilization system that uses photo semiconductor powders, Applied and Environmental Microbiology 54 (1988) 1330–1333.
[41] B. Yu, K.M. Leung, Q. Guo, W.M. Lau, J. Yang, Synthesis of Ag–TiO_2 composite nano thin film for antimicrobial application, Nanotechnology 22 (2011) 115603–115609.
[42] R. Vinu, G. Madras, Environmental remediation by photocatalysis, Journal of the Indian Institute of Sciences 90 (2010) 189–230.